# ANALYTICAL MODEL OF NONLINEAR THERMO-ACOUSTIC EFFECTS IN A MATRIX BURNER

Maria A. Heckl

Department of Mathematics, Keele University
Staffordshire ST5 5BG, UK
m.a.heckl@keele.ac.uk

This paper considers a fundamental thermo-acoustic test rig developed by Noiray ("Linear and nonlinear analysis of combustion instabilities, application to multipoint injection systems and control strategies", PhD thesis, École Centrale Paris, 2007). The main components of this test rig are a resonant duct of variable length, terminated by a moveable piston at the upstream end and a perforated plate at the downstream end; a two-dimensional array of small premixed flames is anchored just outside the duct by the perforated plate. We model this with an entirely analytical approach. The flame describing function measured by Noiray is represented by a heat release law with two time-lags, and this law is then used to derive the governing equation for a single acoustic mode in the test rig. This equation turns out to be that of a harmonic oscillator with a damping/amplification coefficient that depends on the velocity amplitude. On this basis we find analytically the pattern of the oscillation regimes in parameter space, in particular the frequency and amplitude of limit cycles at various tube lengths. There is good qualitative agreement with Noiray's observations. The paper concludes by exploring generic heat release laws with multiple and/or distributed time-lags; the corresponding features in the flame transfer function are discussed.

## 1 Introduction

Nonlinear effects in a thermo-acoustic system lead to interesting behaviours, such as limit cycles or hysteresis effects. These have been observed by a number of researchers, in particular by Noiray [1], who studied a fundamental test rig from an experimental perspective. The aim of our paper is to present a more analytical approach so as to shed light on the role of certain nonlinear mechanisms.

The main components of Noiray's test rig are shown in Figure 1.

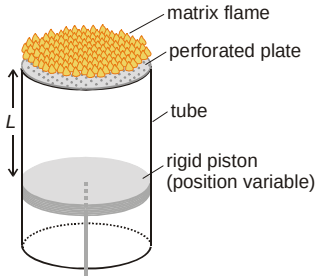


Figure 1: Noiray's matrix burner.

A resonant tube of variable length is terminated by a moveable piston at the upstream end and by a perforated plate at the downstream end. A two-dimensional array (matrix) of small premixed flames is anchored just outside the tube at the perforated plate. Essentially, the tube is a quarter-wave resonator (one rigid and one nearly open end).

# 2 Flame describing function

## 2.1 Measured results

Noiray determined an experimental "flame describing function" (FDF) by measuring the flame transfer function (FTF) for a range of velocity amplitudes. His results for the gain and phase have been reproduced in Figures 2 (a, b).

(a)

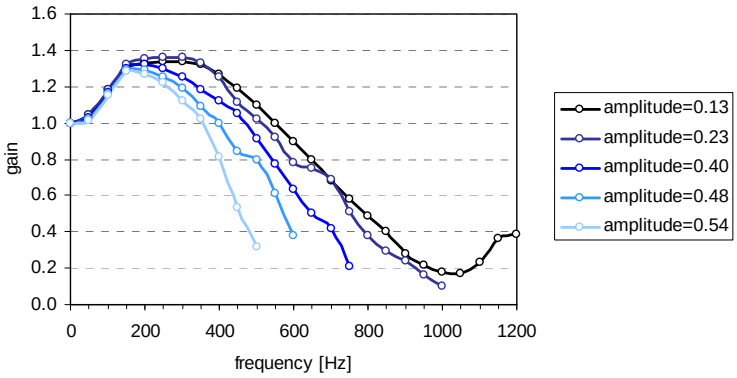


(b)

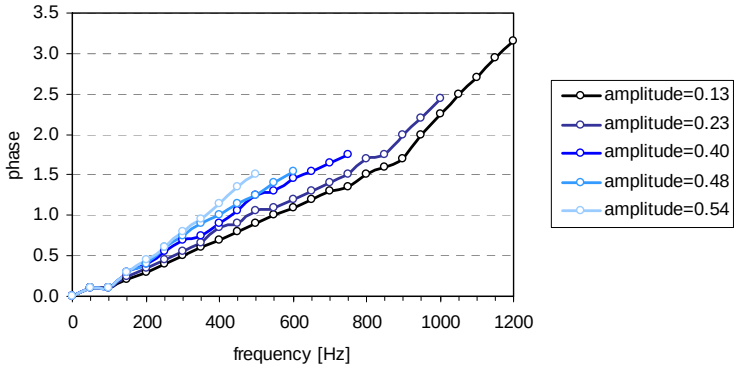


Figure 2: Measured FDF for different velocity amplitudes (normalised with the mean velocity) (a) gain. (b) phase.

The following features are notable.
(1) In the gain curves, there are two effects as the amplitude increases:
  (a) The frequency interval, which spans the first minimum (at zero frequency) to the next minimum becomes smaller.
  (b) The gain maximum becomes smaller.
(2) The slope of the phase curves increases as the amplitude increases.

## 2.2 Analytical description

Our starting point is the hypothetical heat release law in the time domain,

$$\frac{Q(t)}{\bar{Q}} = n_1 \frac{u(t-\tau)}{\bar{u}} - n_0 \frac{u(t)}{\bar{u}}\,, \tag{1}$$

where

$\bar{Q}$ : rate of heat release, mean part

$Q$ : rate of heat release, fluctuating part

$\bar{u}$ : velocity, mean part

$u$ : velocity, fluctuating part

$n_1, n_2$ : real positive parameters

This heat release law has a time-lagged component and an instant component. Its frequency-domain equivalent is

$$\frac{\hat{Q}(\omega)}{\bar{Q}} = (n_1 e^{i\omega\tau} - n_0)\frac{\hat{u}(\omega)}{\bar{u}}, \tag{2}$$

which gives the FTF, $\mathcal{T}(\omega)$, as

$$\mathcal{T}(\omega) = n_1 e^{i\omega\tau} - n_0 . \tag{3}$$

The gain of this FTF,

$$|\mathcal{T}(\omega)| = \sqrt{n_0^2 + n_1^2 - 2n_0 n_1 \cos\omega\tau}\ , \tag{4}$$

is a periodic function of $\omega\tau$ with a minimum at $\omega\tau = 0$, followed by a maximum at $\omega_{max}\tau = \pi$ and a subsequent minimum at $\omega_{min}\tau = 2\pi$.

The phase of this FTF is

$$\arg\mathcal{T}(\omega) = \frac{n_1 \sin\omega\tau}{n_1\cos\omega\tau - n_0} \approx \frac{n_1}{n_1 - n_0}\omega\tau\ ; \tag{5}$$

the last step in (5) is an approximation for small frequencies, and this indicates that, at small frequencies, the slope of the phase curve is proportional to the time-lag $\tau$.

In order to fit our analytical $\mathcal{T}(\omega)$ to the measured curves in Figure 2, we chose

$$n_1 - n_0 = 1 \quad \text{(this gives a gain of 1 at } \omega = 0) \tag{6a}$$

$$n_1 + n_0 = g_{max} \quad \text{(this gives a gain of } g_{max} \text{ at the 1st maximum)} \tag{6b}$$

The gain measured at the smallest amplitude is shown by the black curve in Figure 2(a). For this curve, we have $g_{max} \approx 1.34$ and $\omega_{min} \approx 2\pi \cdot 1050\ s^{-1}$. The latter result gives $\tau = 0.00095$ s. This agrees with the value obtained from the corresponding phase curve in Figure 2(b). At higher amplitudes, both the time-lag $\tau$ and the gain-maximum $g_{max}$ change. The $g_{max}$ values can be read off Figure 2.1(a) directly, and the $\tau$ values can be estimated by extrapolating the gain curves to their second minimum. Table 1 shows the values for Noiray's five amplitudes.

| $A/\bar{u}$ | $g_{max}$ | $f_{min}$ [Hz] | $\tau$ [$10^{-3}$ s] |
|---|---|---|---|
| 0.13 | 1.34 | 1050 | 0.95 |
| 0.23 | 1.36 | 1010 | 0.99 |
| 0.40 | 1.32 | 850 | 1.18 |
| 0.48 | 1.29 | 650 | 1.54 |
| 0.54 | 1.28 | 550 | 1.82 |

Table 1: FDF properties for increasing velocity amplitudes $A$.

The data in Table 1 has been used to generate Figures 3(a) and 3(b), which show the amplitude-dependence of the time-lag and of the gain-maximum, respectively.

(a)

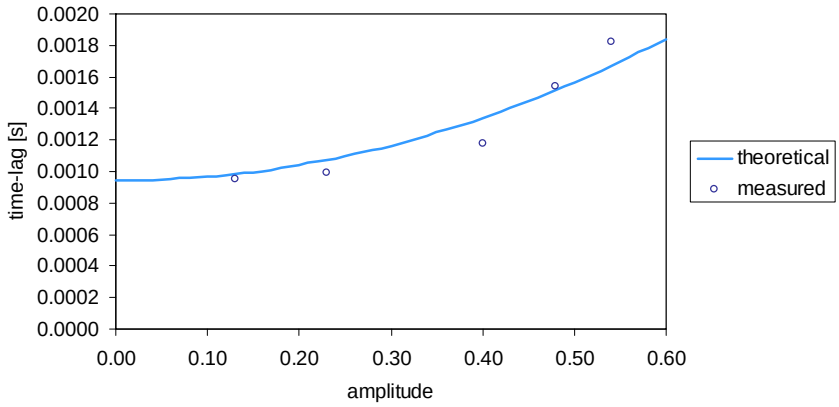


(b)

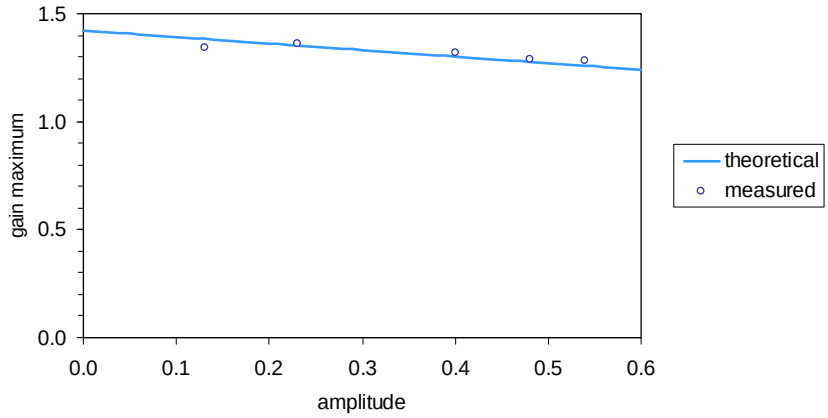


Figure 3: Dependence on velocity amplitude of (a) time-lag. (b) gain-maximum.

The data points for the time-lag lie on a curve with growing slope. We approximate them analytically by a parabola, whose vertex is at the point $(0,\tau_0)$, i.e. by

$$\tau = \tau_0 + \tau_2 (\frac{A}{\bar{u}})^2 . \tag{7}$$

For the constants $\tau_0$ and $\tau_2$ we chose

$$\tau_0 = 0.94 \cdot 10^{-3}\,\mathrm{s}\,,\ \tau_2 = 2.5 \cdot 10^{-3}\,\mathrm{s}\,, \tag{8a,b}$$

because this gives reasonable agreement with the measured data, as shown in Figure 3(a).

The data points for the gain maximum are somewhat irregular, but show an overall decreasing trend. We approximate them analytically by a line with a negative slope, i.e. by

$$g_{\max} = g_0 - g_1 \frac{A}{\bar{u}} . \tag{9}$$

For the constants $g_0$ and $g_1$ we chose

$$g_0 = 1.42\,,\ g_1 = 0.3\,, \tag{10a,b}$$

because this gives reasonable agreement with the measured data, as shown in Figure 3(b).

Figure 4 shows the gain and phase of our analytical FDF, which is based on (3) and represented by

$$\mathcal{T}(\omega, A) = n_1(\mathrm{A})\mathrm{e}^{\mathrm{i}\omega\tau(A)} - n_0(A) \tag{11}$$

with

$$n_1(A) = \frac{1}{2}[g_{max}(A)+1]\,,\quad n_0(A) = \frac{1}{2}[g_{max}(A)-1]\,. \tag{12a,b}$$

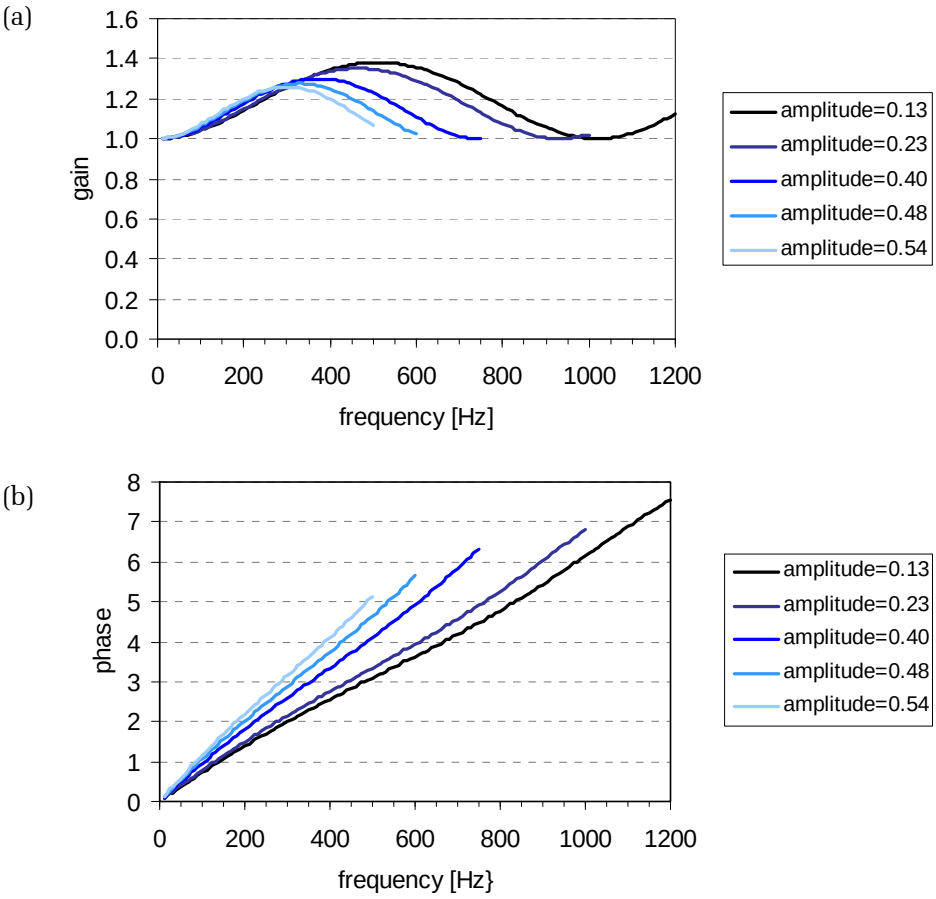


Figure 4: Analytical FDF given by (11) with (7)-(10) and (12). (a) gain. (b) phase.

Comparison with Figure 2 shows that our analytical representation captures the following key features of the measured FDF.

(1) The position of the maximum and subsequent minimum in the gain curves moves to smaller frequency values as the amplitude increases.

(2) The slope of the phase curve (which for small frequencies is proportional to $\tau$), increases as the amplitude increases.

(3) The value of the gain maximum decreases as the amplitude increases.

Not captured in our assumptions is the low-pass behaviour of the measured FDF, which leads to a reduction in gain at higher frequency values.

# 3 The governing equations

## 3.1 Model for the combustor

We assume purely one-dimensional conditions. The acoustic field in the tube consists of backward and forward travelling waves, as shown in Figure 5. These are reflected at the upstream end by the piston (reflection coefficient $R_0$), and at the downstream end by the combined boundary represented by the perforated plate and open end,

$$R_L = \frac{R_{pp} - R_{pp}^2 R_{oe} + T_{pp}^2 R_{oe}}{1 - R_{pp} R_{oe}}, \tag{13}$$

$$T_L = \frac{T_{pp} T_{oe}}{1 - R_{pp} R_{oe}}, \tag{14}$$

where $R_{pp}$ and $T_{pp}$ are the reflection and transmission coefficient, respectively, of the perforated plate, and $R_{oe}$ and $T_{oe}$ are those for an unflanged open tube end (for details, see [2]).

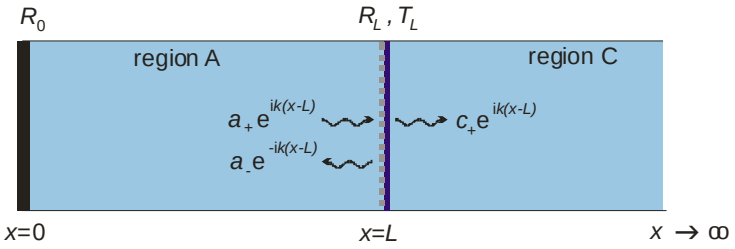


Figure 5: The modelled configuration.

We ignore the fact that the sound wave transmitted beyond the downstream tube end becomes three-dimensional, and instead assume that the tube has a semi-infinite continuation, which keeps the transmitted wave one-dimensional. We also assume that the mean temperature is uniform everywhere in the tube. The speed of sound (denoted by $c$) is constant.

The eigenfrequencies $\omega_n$ of this configuration are given by

$$F(\omega) = \mathrm{e}^{-\mathrm{i}\omega L/c} - R_0 R_L \mathrm{e}^{\mathrm{i}\omega L/c} = 0. \tag{15}$$

We are going to use a Green's function approach, which requires the tailored Green's function. This is given by a superposition of modes $n$,

$$G(t,t') = \mathrm{H}(t-t') \sum_{n=1}^{\infty} \mathrm{Re}[G_n \mathrm{e}^{-\mathrm{i}\omega_n (t-t')}], \tag{16}$$

where $t$ and $t'$ are observer and source time, respectively, $\mathrm{H}(t-t')$ is the Heaviside function (this guarantees causality), the amplitudes $G_n$ are given by

$$G_n = -\frac{c}{2L} R_0 T_L^2 \mathrm{e}^{2\mathrm{i}\omega_n x_q/c}, \tag{17}$$

and $x_q$ is the axial position of the matrix flame.

## 3.2 Governing equation for a single mode

The mathematical steps in the derivation of this equation are lengthy and complex; details can be found in [2]. Here we just give a few highlights.

The flame in the combustor is considered to be compact, and a Green's function approach is employed to derive an integral equation for the acoustic velocity. This is

$$u(t) = \frac{B}{2} \int_{t'=0}^{t} \sum_{n=1}^{\infty} [G_n \mathrm{e}^{-\mathrm{i}\omega_n (t-t')} + G_n^* \mathrm{e}^{\mathrm{i}\omega_n^* (t-t')}]\, q(t')\, dt' \tag{18}$$

where $B = -(\gamma - 1)/c^2$ is an abbreviation, and $\gamma$ denotes the specific heat ratio. $q(t)$ is the local rate of heat release, and it is proportional to its global counterpart $Q'(t)$,

$$q(t) = \alpha\left[n_1 u(t-\tau) - n_0 u(t)\right], \tag{19}$$

with $\alpha = \overline{Q}/(\overline{u}\overline{\rho}\mathcal{A})$, where $\overline{\rho}$ is the mean density.

A single mode $n$ can be considered by dropping the summation sign in (18). The resulting equation can be converted to an ODE for $u(t)$, and the result is

$$\ddot{u} - 2\,\mathrm{Im}(\omega_n)\dot{u} + |\,\omega_n\,|^2\, u = -B\,\mathrm{Im}(\omega_n G_n^*)q(t) + B\,\mathrm{Re}(G_n)\dot{q}(t)\,. \tag{20}$$

### 3.3 Interpretation

Equation (20) is the ODE for a forced harmonic oscillator. It is the governing equation for the acoustic velocity $u(t)$, forced by the heat release rate $q(t)$ and its time derivative $\dot{q}(t)$. Substitution of (19) into (20) leads to

$$\ddot{u}(t) + c_1\dot{u}(t) + c_0 u(t) = b_0 u(t-\tau) + b_1\dot{u}(t-\tau)\,, \tag{21}$$

with

$$b_0 = -\alpha n_1 B\,\mathrm{Im}(\omega_n G_n^*)\,,\ b_1 = \alpha n_1 B\,\mathrm{Re}(G_n)\,, \tag{22a,b}$$

$$c_0 = |\,\omega_n\,|^2 - \alpha n_0 B\,\mathrm{Im}(\omega_n G_n^*)\,,\ c_1 = -2\,\mathrm{Im}(\omega_n) + \alpha n_0 B\,\mathrm{Re}(G_n)\,. \tag{22c,d}$$

The time-lag is not necessarily small, in fact it can become larger than the period of the oscillation. We assume that $u(t)$ is sinusoidal with frequency $\Omega$ and amplitude $A$, and express the time-lag terms in terms of $u(t)$ and $\dot{u}(t)$. This gives

$$u(t-\tau) = A\cos\Omega(t-\tau) = (\cos\Omega\tau)\,u(t) - \frac{\sin\Omega\tau}{\Omega}\,\dot{u}(t)\,, \tag{23}$$

$$\dot{u}(t-\tau) = (\Omega\sin\Omega\tau)\,u(t) + (\cos\Omega\tau)\,\dot{u}(t)\,, \tag{24}$$

and (21) can be written as

$$\ddot{u}(t) + [c_1 + b_0\frac{\sin\Omega\tau}{\Omega} - b_1\cos\Omega\tau]\,\dot{u}(t) + [c_0 - b_0\cos\Omega\tau - b_1\Omega\sin\Omega\tau]\,u(t) = 0\,. \tag{25}$$

Clearly, this is the equation for a damped harmonic oscillator. The damping coefficient is

$$a_1 = c_1 + b_0\frac{\sin\Omega\tau}{\Omega} - b_1\cos\Omega\tau\,, \tag{26}$$

and the other coefficient,

$$a_0 = c_0 - b_0\cos\Omega\tau - b_1\Omega\sin\Omega\tau \tag{27}$$

is the square of the oscillation frequency. The amplitude-dependence comes in through the time-lag (see (7)), which appears explicitly in (7), and through the gain-maximum (see (9)), which determines the coefficients $n_0$ and $n_1$ in (19).

It is instructive to examine the values of $a_1$ for an array of parameter values for $L$ and $A$. Contours of $a_1(L,A) = 0$ in the $LA$-plane indicate steady oscillations, i.e. limit cycles.

# 4 Results for the stability behaviour

## 4.1 Measured results

We reproduced the stability map measured by Noiray; this is shown in Figure 6. Blue (pale grey) regions indicate stability, and red (dark grey) regions indicate instability. In order to make it easy to compare this map with our predictions, which cover the amplitude range $A/\overline{u} = 0 \ldots 2$, we plotted Noiray's map for the same range. However, Noiray's data is available only for the range $A/\overline{u} = 0 \ldots 0.8$, so the "results" shown in Figure 6 for $A/\overline{u} > 0.8$ are not reliable.

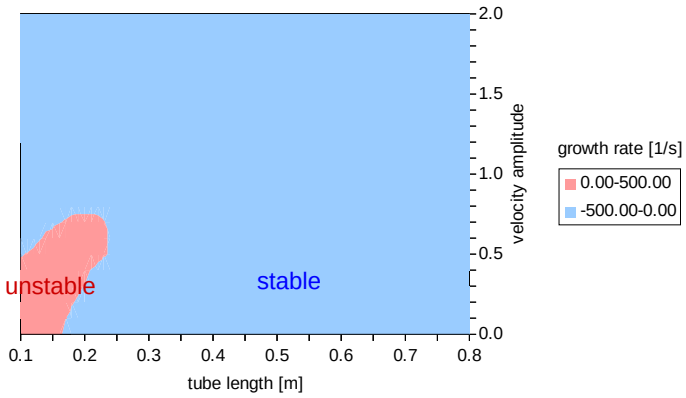


Figure 6: Measured stability map for mode 1.

The unstable region has the shape of a tongue. Linear stability behaviour can be discerned from the behaviour near the $L$-axis. The point $L = 0.17\text{m}$, $A/\overline{u} = 0$ on the map separates the linearly unstable and linearly stable range. This point is a subcritical Hopf bifurcation. Branching off from this point are unstable limit cycles. The point $L = 0.24\text{m}$, $A/\overline{u} = 0.5$, i.e. the "tip of the tongue", is a fold point. It separates unstable limit cycles from stable ones. The region between $L = 0.17\text{m}$ and $L = 0.24\text{m}$ is a bi-stable region, where hysteresis can be observed.

## 4.2 Predicted results

We consider the fundamental mode of the tube and choose parameters in line with the actual values of Noiray's setup:

$a = 0.035\,\text{m}$ (tube radius)
$L = 0.1\,\text{m} \ldots 0.8\,\text{m}$ (range of tube lengths)
$h = 0.003\,\text{m}$ (thickness of perforated plate)
$\mathcal{N} = 1.09 \cdot 10^5\,\text{m}^{-2}$ (number of perforations per unit area)
$r_p = 0.001\,\text{m}$ (radius of perforations)
$c = 345\,\text{ms}^{-1}$ (speed of sound)
$\gamma = 1.4$ (specific heat ratio)
$\alpha = 3 \cdot 10^5\,\text{m}^2\text{s}^{-2}$ (factor relating $q(t)$ and $Q(t)$)
$x_q - L = 0.01\,\text{m}$ (distance of flame from perforated plate)
$R_0 = 1$ (pressure reflection coefficient at the piston)

The amplitude-dependence of the time-lag and gain-maximum are described by (7) and (9) respectively, with the parameter values given in (8a,b) and (10a,b).

Figure 7 shows the predicted stability map on the same scale as Figure 6. The unstable regions have the shape of a curved band. There is one main band, which spans the whole $L$-range. Above that, there are 3 minor bands with decreasing width.

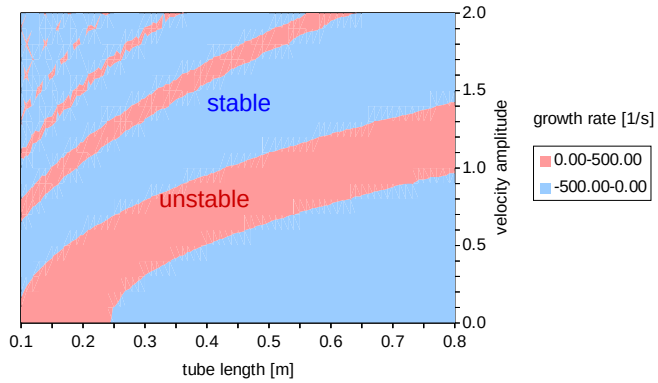


Figure 7: Predicted stability map.

These predictions capture the behaviour at low amplitudes, in particular the linear stability range and the limit cycle amplitudes for low $L$-values. However, there is a major discrepancy: our model predicts a *band* of instability, which spans the whole $L$-range, whereas Noiray's instability region has the shape of a *tongue*, which does not extend beyond $L$-values of 0.25 m.

The four parameters $\tau_0, \tau_2, g_0, g_1$, which characterise the amplitude-dependence of the FDF, have a strong influence on the shape of the instability region. In particular, reducing $g_0$ and increasing $g_1$ (which amounts to reducing the overall gain), turns the main band in Figure 7 into a tongue. This is shown in Figure 8.

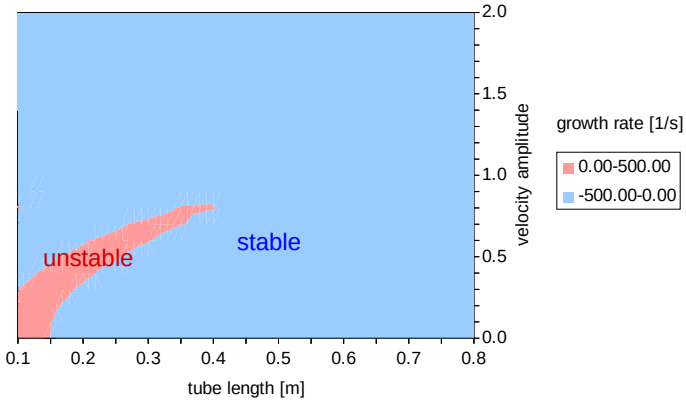


Figure 8: Predicted stability map for $g_0 = 1, g_1 = 0.4$.

The predicted stability map in Figure 8 has all the features as its experimental counterpart in Figure 6. This indicates that our model works well, but that our original gain values were overestimates. Our simulations also showed that both time-lag *and* gain maximum must be amplitude-dependent; the time-lag on its own fails to predict the observed fold point.

# 5 Summary and outlook

## 5.1 Summary

We approximated the FTF measured by Noiray by an FTF derived from the heat release law

$$\frac{Q(t)}{\bar{Q}} = n_1 \frac{u(t-\tau)}{\bar{u}} - n_0 \frac{u(t)}{\bar{u}} . \tag{28}$$

The measured FDF was based on (28), too, with the amplitude dependence simulated by

- a time-lag $\tau$ that increases with amplitude, and
- a gain maximum $n_1 + n_0$ that decreases with amplitude.

Our predicted stability map gave good agreement at low amplitudes. However, in order to get good agreement at higher amplitudes as well, it was necessary to reduce the gain artificially. This indicates that the gain has been over-estimated, which is indeed the case, given that the low-pass behaviour of the measured FTF has not been included in our model.

Some earlier authors have found the concept of multiple time-lags useful. For example, in various studies led by Polifke [3-8], the following observations were made.
- Multiple time-lags can lead to excess gain.
- A fluctuation "smears out" during its passage through the burner, leading to a distribution of time-lags, which in turn leads to an FTF with low-pass characteristic.

The aim of the next two subsections is to explore the consequences of multiple time-lags, and in particular to identify the features that are responsible for the low-pass characteristic of an FTF. Section 5.2 considers discrete time-lags, and section 5.3 considers continuous distributions of time-lags.

## 5.2 Heat release law with discrete time-lags

We extend (28) by adding more time-lag terms,

$$\frac{Q(t)}{\bar{Q}} = n_0 \frac{u(t)}{\bar{u}} + n_1 \frac{u(t-\tau_1)}{\bar{u}} + n_2 \frac{u(t-\tau_2)}{\bar{u}} + \dots \tag{29}$$

where $\tau_1, \tau_2, \dots$ are time-lags (all positive), and $n_0, n_1, n_2, \dots$ are positive or negative real coefficients of order 1. The FTF corresponding to (29) is

$$\mathcal{T}(\omega) = n_0 + n_1 e^{i\omega\tau_1} + n_2 e^{i\omega\tau_2} + \dots \tag{30}$$

The gain $|\mathcal{T}(\omega)|$ is best estimated by representing (30) as a sum of individual vectors in the complex plane and constructing the sum graphically. It can then be seen that $\mathcal{T}(\omega)$ lies within a finite region of the complex plane, that its modulus fluctuates between 0 and $n_0 + n_1 + n_2 + \dots$, and that there is no global decay for large $\omega$.

The phase can be calculated directly if the real and imaginary parts in (30) are separated,

$$\mathcal{T}(\omega) = n_0 + n_1 \cos\omega\tau_1 + n_2 \cos\omega\tau_2 + \dots + i(n_1 \sin\omega\tau_1 + n_2 \sin\omega\tau_2 + \dots). \tag{31}$$

Then

$$\arg\mathcal{T}(\omega) = \frac{n_1 \sin\omega\tau_1 + n_2 \sin\omega\tau_2 + \dots}{n_0 + n_1 \cos\omega\tau_1 + n_2 \cos\omega\tau_2 + \dots}. \tag{32}$$

For small frequencies, this can be approximated by

$$\arg\mathcal{T}(\omega) = \omega \frac{n_1\tau_1 + n_2\tau_2 + \dots}{n_0 + n_1 + n_2 + \dots}, \tag{33}$$

i.e. the phase curve is a straight line whose slope is given by the average time-lag (weighted with the coefficients $n_0, n_1, n_2, \dots$).

## 5.3 Heat release law with time-lag distribution

We start by considering

$$\frac{Q(t)}{\bar{Q}} = \int_{\tau=\tau_k-\Delta\tau/2}^{\tau_k+\Delta\tau/2} n \frac{u(t-\tau)}{\bar{u}} \mathrm{d}\tau. \tag{34}$$

This is a superposition of infinitely many time-lag terms, with time-lags clustered around $\tau_k$, each with the same weighting $n$.

It is convenient to introduce the top-hat function $\Pi_k(\tau)$, defined by

$$\Pi_k(\tau) = \begin{cases} 1 & \text{if} \quad \tau_k - \dfrac{\Delta\tau}{2} < \tau < \tau_k + \dfrac{\Delta\tau}{2} \\ 0 & \text{elsewhere} \end{cases} \tag{35}$$

This is shown in Figure 9.

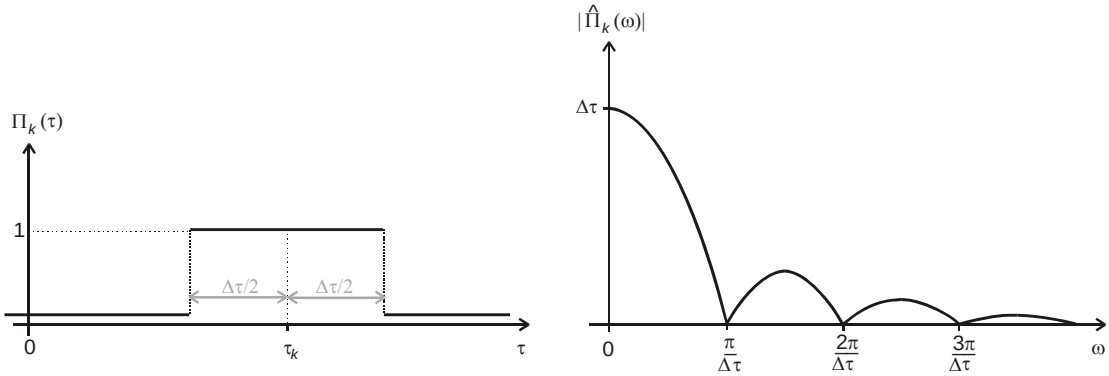


Figure 9: Top-hat function and its Fourier transform (magnitude only).

It has a known Fourier transform (also shown in Figure 9), given by

$$\mathcal{F}[\Pi_k(\tau)] = \hat{\Pi}_k(\omega) = \mathrm{e}^{\mathrm{i}\omega\tau_k}\,\frac{2}{\omega}\sin\frac{\omega\Delta\tau}{2}\,. \tag{36}$$

The most interesting feature for our purposes is the low-pass behaviour of $|\hat{\Pi}_k(\omega)|$.

With the top-hat function, (34) can be written in terms of a convolution integral,

$$\frac{Q(t)}{\bar{Q}} = n\int_{\tau=-\infty}^{\infty} \Pi_k(\tau)\frac{u(t-\tau)}{\bar{u}}\mathrm{d}\tau\,. \tag{37}$$

The Fourier transform of this is

$$\frac{\hat{Q}(\omega)}{\bar{Q}} = n\,\hat{\Pi}_k(\omega)\frac{\hat{u}(\omega)}{\bar{u}}\,, \tag{38}$$

which, with (36), gives the FTF

$$\mathcal{T}(\omega) = n\,\mathrm{e}^{\mathrm{i}\omega\tau_k}\,\frac{2}{\omega}\sin\frac{\omega\Delta\tau}{2}\,. \tag{39}$$

The gain and phase, respectively, of this FTF are

$$|\mathcal{T}(\omega)| = n\,\frac{2}{\omega}\left|\sin\frac{\omega\Delta\tau}{2}\right| \qquad \text{and} \quad \arg\mathcal{T}(\omega) = \tan\omega\tau_k \approx \omega\tau_k\,. \tag{40a,b}$$

The gain is independent of $\tau_k$ and has low-pass behaviour. The phase can be approximated by $\omega\tau_k$ for small frequencies.

We now extend our considerations to the case where there are several distinct time-lags in the heat release law, each surrounded by a distribution of width $\Delta\tau$,

$$\frac{Q(t)}{\bar{Q}} = \int_{\tau=\tau_1-\Delta\tau/2}^{\tau_1+\Delta\tau/2} n_1\frac{u(t-\tau)}{\bar{u}}\mathrm{d}\tau + \int_{\tau=\tau_2-\Delta\tau/2}^{\tau_2+\Delta\tau/2} n_2\frac{u(t-\tau)}{\bar{u}}\mathrm{d}\tau + \ldots \tag{41}$$

The FTF corresponding to that can be easily determined with the superposition principle, and the result is

$$\mathcal{T}(\omega) = \frac{2}{\omega}\sin\frac{\omega\Delta\tau}{2}\left(n_1 e^{i\omega\tau_1} + n_2 e^{i\omega\tau_2} + \dots\right). \tag{42}$$

Its gain

$$|\mathcal{T}(\omega)| = \left|\frac{2}{\omega}\sin\frac{\omega\Delta\tau}{2}\right|\left|n_1 e^{i\omega\tau_1} + n_2 e^{i\omega\tau_2} + \dots\right| \tag{43}$$

shows low-pass behaviour. Its phase is given by

$$\arg\mathcal{T}(\omega) = \frac{n_1\ \sin\omega\tau_1 + n_2\ \sin\omega\tau_2 + \dots}{n_0 + n_1\ \cos\omega\tau_1 + n_2\ \cos\omega\tau_2 + \dots} \approx \omega\frac{n_1\tau_1 + n_2\tau_2 + \dots}{n_0 + n_1 + n_2 + \dots}. \tag{44}$$

Again, for small frequencies, the phase curve is a straight line whose slope is given by the average time-lag (weighted with the coefficients $n_0, n_1, n_2, \dots$ ).

Our findings are in line with those in [3-8].

# References


[1] N. Noiray. *Linear and nonlinear analysis of combustion instabilities, application to multipoint injection systems and control strategies*. PhD thesis, Ecole Centrale Paris. 2007.

[2] M.A. Heckl. Analytical model for nonlinear thermo-acoustic effects in a matrix burner. Accepted for publication in the *Journal of Sound and Vibration*, 2013.

[3] W. Polifke, J. Kopitz and A. Serbanovic. Impact of the fuel time lag distribution in elliptical premix nozzles on combustion stability. *Proceedings of the 7th AIAA/CEAS Aeroacoustics Conference, Maastricht, The Netherlands, 28-30 May 2001* paper AIAA 2001-2104, 2001.

[4] C.J. Lawn and W. Polifke. A model for the thermoacoustic response of a premixed swirl burner -Part II: The flame response. *Combustion Science and Technology* 176: 1359-1390, 2004.

[5] A. Huber and W. Polifke. Dynamics of practical premixed flames, part II: identification and interpretation of CFD data. *International Journal of Spray and Combustion Dynamics* 1: 229 – 250, 2009.

[6] T. Komarek and W. Polifke. Impact of swirl fluctuations on the flame response of a perfectly premixed swirl burner. *Journal of Engineering for Gas Turbines and Power - Transactions of the ASME* 132, paper no 061503, 2010.

[7] L. Tay-Wo-Chong and W. Polifke. Large eddy simulation-based study of the influence of thermal boundary condition and combustor confinement on premix flame transfer functions. *Journal of Engineering for Gas Turbines and Power - Transactions of the ASME* 134, paper no 021502, 2013.

[8] R.S. Blumenthal, P. Subramanian, R.I. Sujith and W. Polifke. Novel perspectives on the dynamics of premixed flames. Accepted for publication in *Combustion and Flame*, 2013.


# Acknowledgements

I am grateful to Professor Wolfgang Polifke for valuable discussions on the topic of heat release laws with multiple and distributed time-lags.